The Astrophysical Journal, 864:95 (6pp), 2018 September 1 https://doi.org/10.3847/1538-4357/aad55e

Formation of Nascent Product N_2O from the Irradiation of O_2 in Icy N_2

Jen-Iu Lo[1], Sheng-Lung Chou[1], Yu-Chain Peng[1], Hsiao-Chi Lu[1], J. F. Ogilvie[2,3], and Bing-Ming Cheng[1]
[1] National Synchrotron Radiation Research Center, 101 Hsin-Ann Road, Hsinchu Science Park, Hsinchu 30076, Taiwan; bmcheng@nsrrc.org.tw
[2] Department of Mathematics, Simon Fraser University, 8888 University Drive, Burnaby, BC V5A1S6, Canada
[3] Escuela de Quimica, Universidad de Costa Rica, Ciudad Universitaria Rodrigo Facio, San Pedro de Montes de Oca, San Jose 11501-2060, Costa Rica
Received 2018 July 6; revised 2018 July 19; accepted 2018 July 19; published 2018 September 4

Abstract

Products O_3, N, NO, NO_2, N_2O, c-$(NO)_2$, and excited states of O_2 were detected after the photolysis of solid O_2 in icy N_2 near 4 K with radiation at 200 nm. The temporal profiles of these products enable the derivation of a mechanism for the photochemical reactions in this system: dissociation of O_2 first-generated O ^{3}P that reacted with nearby N_2 to yield N_2O. Other products resulted from the secondary photolysis of N_2O and the reactions of O with N_2O. The reaction of O with O_2 to form O_3 was impeded by the small concentration of the latter, which requires substantial migration through the N_2 lattice. However, sufficient O_3 was eventually formed to enable detection either directly from O coming from O_2 or indirectly through N_2O. These results enhance our understanding of the evolution of the transformation of oxygen and nitrogen in irradiated ices and have possible astrophysical applications.

Key words: astrobiology – astrochemistry – ISM: molecules – molecular processes

1. Introduction

Gaseous O_2 and N_2 are the most abundant molecules in our terrestrial atmosphere; both gases are thus important for our life. Both molecules are believed to be present also as ices in non-negligible quantities in cold outer space (Bohn et al. 1994; Elsila et al. 1997; Johnson & Jesser 1997; Johnson & Quickenden 1997; Ehrenfreund & van Dishoeck 1998; Cooper et al. 2003), even though these two molecules are extremely difficult to detect in the infrared telescopes (Strobel & Shemansky 1982; Bernstein & Sandford 1999; Sandford et al. 2001; Knauth et al. 2004). Other gaseous molecules, such as H_2O, CO, CO_2, CH_4, CH_3OH, H_2CO, HCN, C_2H_2, NO, NH_3, etc. might condense as mixed ices in cold astrophysical environments (Mumma & Charnley 2011; Boogert et al. 2015). A bombardment with energetic radiation or particles on the mixed-ice analogues is a plausible route to evolution of the complex compounds in the cosmos. To explore energetic irradiation of the mixed-ice analogues, laboratory experiments are currently being undertaken on icy analogues related to mixed samples including the above molecules (Gerakines et al. 1996; Bernstein et al. 1999; Hudson & Moore 2001; Cottin et al. 2003; Sicilia et al. 2012; Muñoz Caro & Dartois 2013; Kaiser et al. 2015; Öberg 2016; Zhu et al. 2018), but few such experiments in this field take into account the role of the mixed ice of O_2 and N_2 (Broida & Peyron 1960; Schnepp & Dressler 1965; Elsila et al. 1997; Materese et al. 2014). We are thus concerned with the role of irradiation for this icy mixture in a cold universe.

In earlier work, we investigated the photochemical reactions of O_2 dispersed in solid neon near 4 K excited with far-ultraviolet light from a synchrotron source (Chou et al. 2018). This earlier work used both visible and near-ultraviolet emission and absorption to provide evidence for the formation of O_3, which was formed from the combination of a fragment oxygen atom with molecular O_2 in the solid environment, as in Equation (1),

$$O + O_2 \rightarrow O_3. \quad (1)$$

The threshold wavelengths for the photolytic dissociation of gaseous O_2 to atomic oxygen in states ^{3}P, ^{1}D, and ^{1}S via separate channels are all greater than 130 nm (Okabe 1978):

$$O_2 + h\nu(\lambda > 130\ \text{nm}) \rightarrow O(^3P) + O(^3P) \quad \lambda_{th} = 242.2\ \text{nm} \quad (2a)$$

$$\rightarrow O(^3P) + O(^1D) \quad \lambda_{th} = 175.0\ \text{nm} \quad (2b)$$

$$\rightarrow O(^3P) + O(^1S) \quad \lambda_{th} = 133.2\ \text{nm}. \quad (2c)$$

We also studied the thresholds of the photolysis of O_2 and of the formation of O_3 from O_2 dispersed in solid neon. The results showed that the wavelengths at these thresholds were both 200 ± 4 nm, corresponding to an energy of 6.20 ± 0.12 eV; this value is 1.08 eV greater than that in the gaseous phase (Lo et al. 2018). In the present work we expanded our investigation to include the photolysis of solid O_2 in N_2-rich ices to further our understanding of photochemical processes involving oxygen in solid state.

2. Experimental

We performed the photochemical experiments at a photochemical end station coupled to undulator beamline BL21A2 at the Taiwan Light Source in National Synchrotron Radiation Research Center (NSRRC); the apparatus is described previously in Chou et al. (2014, 2017) and Lo et al. (2015). We premixed the O_2 and N_2 in the gaseous phase and deposited the mixture gas for 2 hr on a KBr window cooled to near 4 K. After deposition, the solid samples were irradiated with excitation at 200 nm for sequential periods of 10, 30 s, 1, 5, 10, and 30 minutes and an additional 30 minutes. Infrared absorption spectra were obtained between each two consecutive periods of irradiation resulting in spectra that correspond to total accumulative exposures of 10, 40 s, 1.7, 6.7, 16.7, 46.7, and 76.7 minutes. Our analysis was based on difference infrared absorption spectra—a spectrum taken after the irradiation at each exposure period minus the original one before photolysis. In spectra of this kind, lines pointing upward from the baseline are associated with photolysis products and lines pointing downward are due to the depletion of precursors present before photolysis. Excitation of the samples at 200 nm produced a luminescence, which we recorded as emission spectra with our augmented end station for photochemistry during irradiation of the samples (Lo et al. 2014).

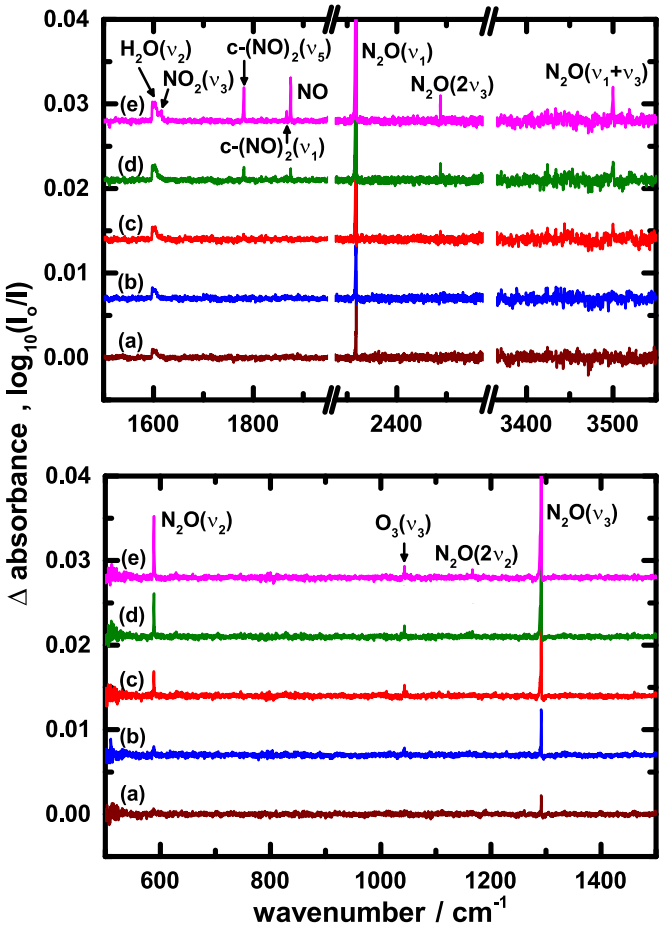

Figure 1. Difference infrared-absorption spectra of O_2 dispersed in solid N_2, 1:500, near 4 K upon excitation at 200 nm for total duration (a) 40 s, (b) 1.7 minutes, (c) 6.7 minutes, (d) 16.7 minutes, and (e) 46.7 minutes. Δabs is the difference of absorbance, $\log_{10}(I_0/I)$. The H_2O bands seen in the spectra are due to small amounts of contaminant in the sample chamber.

The chemical substances in these experiments were O_2 (nominal purity 99.999%, Matheson) and N_2 (nominal purity 99.9999%, Matheson), all used without purification.

3. Results and Discussion

Irradiation at 210 and 220 nm produced emission from O_2, proving that O_2 molecules absorbed that light, but there was no detectable formation of a product. Figures 1(a)–(e) show the difference infrared spectra from O_2 dispersed in solid N_2 (1:500) near 4 K upon excitation at 200 nm for cumulative periods of 0.7, 1.7, 6.7, 16.7, and 46.7 minutes, respectively. These spectra reveal the presence of photolysis products as follows: O_3 at 1043.1 cm^{-1} (ν_3) (Andrews & Spiker 1972; Bahou et al. 1997), NO at 1874.8 cm^{-1} (Broida & Peyron 1960), NO_2 at 1615.9 (ν_3) and 2910.6 ($\nu_1+\nu_3$) cm^{-1}. (Louis & Crawford 1965), cis dimer $(NO)_2$ at 1779.8 (ν_5) and 1866.2 (ν_1) cm^{-1} (Guillory & Hunter 1969), and N_2O at 588.1 (ν_2), 1166.7 ($2\nu_2$), 1291.1 (ν_3), 2235.3 (ν_1), 2575.3 ($2\nu_3$), and 3499.1 ($\nu_1+\nu_3$) cm^{-1} (Sodeau & Withnall 1985). Table 1 lists the observed vibrational wavenumbers and assigned modes of these species. Besides above lines, the lines from contaminants H_2O and CO_2 were present in vestigial proportions; those weak lines are well known without perturbation in these experiments.

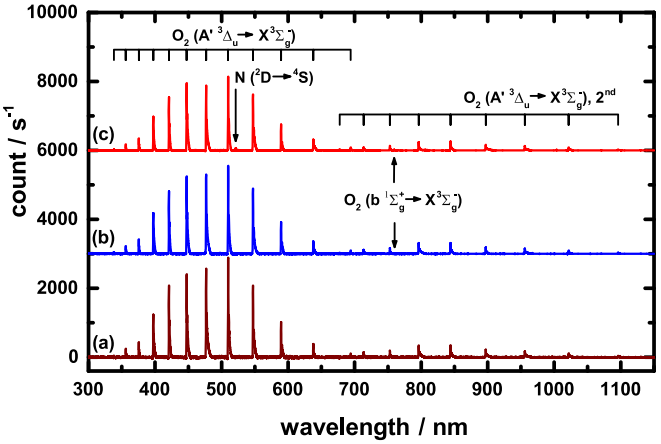

Figure 2. Emission spectra from O_2 dispersed in solid N_2, 1:500, near 4 K upon excitation at 200 nm for (a) 1.7 minutes, (b) 16.7 minutes, and (c) 46.7 minutes.

Figures 2(a)–(c) display emission spectra of O_2 dispersed in solid N_2 (1:500) near 4 K at accumulated periods 1.7, 16.7, and 46.7 minutes, respectively, in the spectral range of 300–1200 nm. At each cumulative period of irradiation, the vibrational progression (v', v'') of O_2 for transition $A'^3\Delta_u \rightarrow X^3\Sigma_g^-$ was recorded from (0, 3) to (0, 14) at 338.2, 355.9, 375.6, 397.4, 421.0, 447.5, 476.7, 509.9, 547.2, 589.4, 637.9, and 694.1 nm (Linstrom & Mallard 2016), respectively; a weak series in the second order of the grating was recorded from (0, 3) to (0, 11) at 677.4, 713.5, 752.9, 796.3, 844.0, 897.2, 955.8, 1021.7, and 1096.0 nm, respectively, as listed in Table 2. We also observed an emission line at 759.3 nm, which is associated with O_2 for the transition $b^1\Sigma_g^+ \rightarrow X^3\Sigma_g^-$ (Linstrom & Mallard 2016). An emission line of atomic N in transition $^2D \rightarrow {}^4S$ was detected at 521.5 nm for cumulative period 46.7 minutes of irradiation (Kramida et al. 2016), but not before.

To track the temporal profiles for the formation of photolysis products, we integrated the intensities of representative lines of O_3 at 1043.1 cm^{-1} (ν_3), NO at 1874.8 cm^{-1}, NO_2 at 1615.9 cm^{-1} (ν_3), c-$(NO)_2$ at 1779.8 (ν_5), and N_2O at 2235.3 cm^{-1} (ν_1) after each cumulative period, also listed in Table 1. Based on these integrated areas, the temporal profiles of products O_3, NO, NO_2, N_2O, and c-$(NO)_2$ are displayed in Figure 3(a); the value for N_2O is divided by 20. The products show distinct temporal characteristics. N_2O appeared immediately, being discernible at 10 s, O_3 appeared at 1.7 minutes, c-$(NO)_2$ at 6.7 minutes, NO at 16.7 minutes, and NO_2 at 46.7 minutes. The temporal profiles of the emission of O_2, $b^1\Sigma_g^+ \rightarrow X^3\Sigma_g^-$ and $A'^3\Delta_u \rightarrow X^3\Sigma_g^-$, and N, $^2D \rightarrow {}^4S$, represented by the integrated areas of the characteristic emission lines are displayed in Figure 3(b).

To understand the mechanisms involved in this photochemical system, we compared this photochemistry with several other systems, namely with O_2 dispersed in solid neon and with pure solid N_2. The photolysis of pure O_2 has been reported but provides no useful information for our purposes (Raut et al. 2011). Figures 4(a)–(c) show the difference infrared spectra of samples near 4 K of O_2 dispersed in solid N_2 (1:500), O_2 dispersed in solid neon (1:500), and pure solid N_2, respectively, after irradiation at 200 nm for a cumulative period of 76.7 minutes. Apart from infrared lines due to minor

Table 1
Observed Vibrational Wavenumbers and Assigned Modes of Products from the Photolysis of O_2 Dispersed in Solid N_2 (1:500) near 4 K upon Irradiation at 200 nm and Integrated Areas of Selected Lines of Products at the Cumulative Photolysis Periods

Species	Observed Vibrational Wavenumber/cm^{-1} (mode)
O_3[a]	1043.1 (ν_3)
NO[b]	1874.8
NO_2[c]	1615.9 (ν_3), 2910.6 ($\nu_1+\nu_3$)
N_2O[d]	588.1 (ν_2), 1166.7 ($2\nu_2$), 1291.1 (ν_3), 2235.3 (ν_1), 2575.3 ($2\nu_3$), 3499.1 ($\nu_1+\nu_3$).
c-$(NO)_2$[e]	1779.8 (ν_5), 1866.2 (ν_1)

Species	Wavenumber (mode)	Integrated Area of Selected Line at Cumulative Photolysis Period						
		10 s	40 s	1.7 minutes	6.7 minutes	16.7 minutes	46.7 minutes	76.7 minutes
N_2O[a]	2235.3 (ν_1)	0.0041	0.0165	0.0373	0.0984	0.1565	0.2301	0.2544
O_3[b]	1043.1 (ν_3)	⋯	⋯	0.0010	0.0013	0.0014	0.0015	0.0017
c-$(NO)_2$[c]	1779.8 (ν_5)	⋯	⋯	⋯	0.0014	0.0030	0.0072	0.0121
NO[d]	1874.8	⋯	⋯	⋯	⋯	0.0012	0.0070	0.0118
NO_2[e]	1615.9 (ν_3)	⋯	⋯	⋯	⋯	⋯	0.0001	0.0013

Notes.
[a] Bahou et al. (1997).
[b] Broida & Peyron (1960).
[c] Louis & Crawford (1965).
[d] Sodeau & Withnall (1985).
[e] Guillory & Hunter (1969).

Table 2
Emission Lines Recorded during Irradiation of O_2 Dispersed in N_2 (1:500) near 4 K Upon Excitation at 200 nm

Species	Transition System	λ/nm	ν/cm^{-1}	$\Delta\nu$/cm^{-1}	v', v''
O_2	$A'^3\Delta_u \rightarrow X^3\Sigma_g^-$	338.2	29567	⋯	(0, 3)
		355.9	28095	1472	(0, 4)
		375.6	26623	1471	(0, 5)
		397.4	25167	1457	(0, 6)
		421.0	23755	1411	(0, 7)
		447.5	22347	1408	(0, 8)
		476.7	20978	1370	(0, 9)
		509.9	19613	1364	(0, 10)
		547.2	18273	1340	(0, 11)
		589.4	16966	1307	(0, 12)
		637.9	15676	1290	(0, 13)
		694.1	14408	1268	(0, 14)
O_2 (second order)	$A'^3\Delta_u \rightarrow X^3\Sigma_g^-$	677.4	14762	⋯	(0, 3)
		713.5	14015	747	(0, 4)
		752.9	13281	733	(0, 5)
		796.3	12557	724	(0, 6)
		844.0	11848	709	(0, 7)
		897.2	11146	702	(0, 8)
		955.8	10463	684	(0, 9)
		1021.7	9788	675	(0, 10)
		1096.0	9124	664	(0, 11)
O_2	$b^1\Sigma_g^+ \rightarrow X^3\Sigma_g^-$	759.3	13170	⋯	(0, 0)
N	$^2D \rightarrow {}^4S$	521.5	19175	⋯	⋯

amounts of contaminant H_2O that were observed in all three photochemical systems, no new infrared line was recorded from the pure solid N_2 sample. O_2 dispersed in solid neon only produced O_3, evidenced by lines at 1038.7 and 1039.7 cm^{-1} (ν_3). In contrast, infrared lines of photolysis products O_3, NO, NO_2, N_2O, and c-$(NO)_2$ were observed from O_2 dispersed in solid N_2, as mentioned above. Thus, the addition of N_2 to the O_2 clearly yields a much richer photochemistry.

What, then, are the nascent photolysis products from these two photochemical systems? Figures 5(a) and (b) display the difference infrared spectra from O_2 dispersed in solid N_2 (1:500) and O_2 dispersed in solid neon (1:500), respectively, after irradiation at 200 nm for a cumulative period of 40 s. At the nascent photolysis stage, only product N_2O was observed from O_2 dispersed in solid N_2, whereas O_3 was generated from O_2 dispersed in solid neon. The photolysis threshold of solid N_2 to form N_3 is at 145.6 nm (Chou et al. 2014; Lo et al. 2015), therefore, the product N_2O generated at 200 nm does not require N_3 from solid N_2 as an intermediary.

In our preceding work, we determined the thresholds of photolysis of O_2 and of the formation of O_3 from O_2 dispersed in solid neon both to be 200 ± 4 nm, corresponding to an energy of

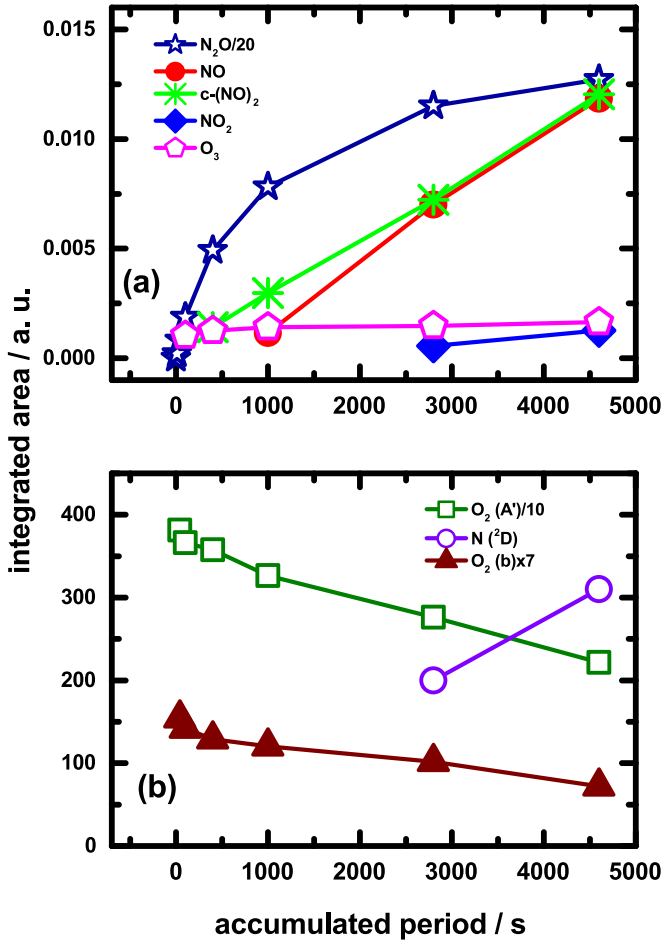

Figure 3. For O_2 dispersed in solid N_2 (1:500) near 4 K irradiated at 200 nm, (a) temporal profiles of formation of O_3, NO, NO_2, N_2O, and c-$(NO)_2$, according to the integrated area of characteristic infrared-absorption lines (the strengths of the other bands for NO_2, N_2O, and c-$(NO)_2$ are consistent with the shape of the plotted curves) and (b) temporal profiles of O_2 (b), O_2 (A'), and N (^{2}D) represented by the integrated area of characteristic emission lines.

6.20 ± 0.12 eV (Lo et al. 2018); this value is 1.08 eV greater than for the gaseous phase. This result indicates that separate O (^{3}P) atoms can be generated and can react with O_2 to form O_3, according to Equation (1), at 200 nm in solid neon. From Figure 5, the nascent product in solid N_2 on irradiation at 200 nm is N_2O. In a N_2 matrix, we hence propose that fragment O (^{3}P) atoms first react with a host molecule N_2 nearby to form the nascent product N_2O,

$$O(^3P) + N_2 \rightarrow N_2O. \quad (3)$$

In the gaseous phase, dinitrogen monoxide (N_2O) is dissociated photochemically according to these channels (Atkinson et al. 1997):

$$N_2O + h\nu \rightarrow N_2 + O(^3P) \quad \lambda_{th} = 742\ \text{nm} \quad (4a)$$
$$\rightarrow N_2 + O(^1D) \quad \lambda_{th} = 341\ \text{nm} \quad (4b)$$
$$\rightarrow NO + N(^4S) \quad \lambda_{th} = 252\ \text{nm} \quad (4c)$$
$$\rightarrow N_2 + O(^1S) \quad \lambda_{th} = 212\ \text{nm}. \quad (4d)$$

The quantum yield to produce O (^{1}D) from the photolysis of gaseous N_2O in the 185–230 nm wavelength region, as in Equation 4(b), has been recommended to have a value of 1.0 (Raut et al. 2011). We thus assume that channel 4(b) in solid N_2 is the most favorable route upon irradiation at 200 nm to form

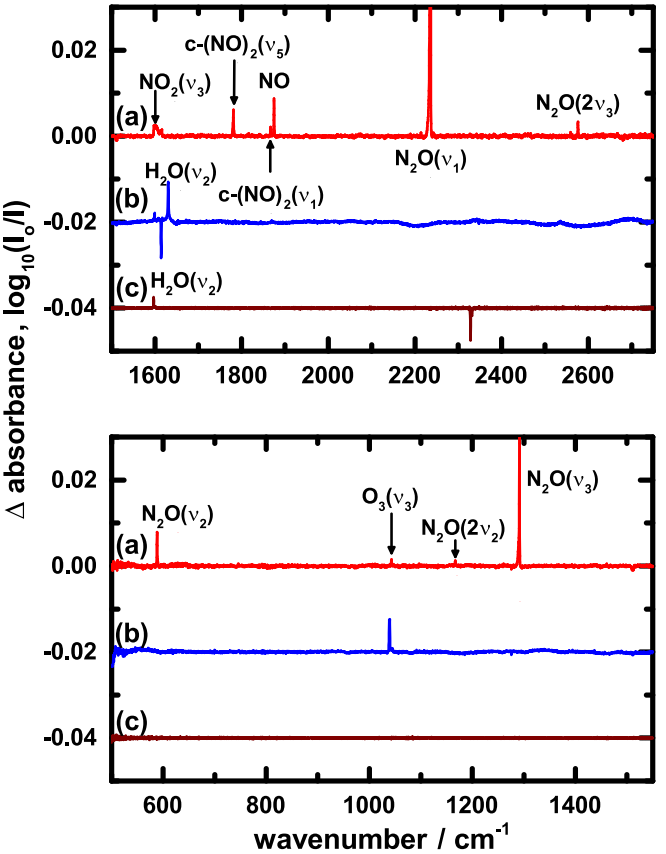

Figure 4. Difference infrared-absorption spectra after irradiation at 200 nm for 76.7 minutes near 4 K from (a) O_2 dispersed in solid N_2, 1:500; (b) O_2 dispersed in solid neon, 1:500; and (c) pure solid N_2. Δabs is the difference of absorbance, $\log_{10}(I_0/I)$.

N_2 + O (^{1}D) in solid N_2. The reactive O (^{1}D) atoms generated in solid N_2 subsequently react with N_2 and N_2O as follows (Atkinson et al. 1997):

$$O(^1D) + N_2 \rightarrow N_2 + O(^3P) \quad (5)$$
$$O(^1D) + N_2O \rightarrow N_2O + O(^3P) \quad (6a)$$
$$\rightarrow N_2 + O_2 \quad (6b)$$
$$\rightarrow (NO)_2 \quad (6c)$$
$$\rightarrow 2NO. \quad (6d)$$

Atomic O (^{1}D) can also react with side product NO to generate product NO_2 as

$$O(^1D) + NO \rightarrow NO_2. \quad (7)$$

In addition, all O (^{1}D), O (^{3}P), and O (^{1}S) atoms might react with O_2 to produce O_3 as in Equation (1) in this photochemical system. Once ozone is produced, it is readily susceptible to dissociation to produce atomic O and molecule O_2 as discussed in our previous work (Chou et al. 2018; Lo et al. 2018).

As discussed above, products O_3, NO, c-$(NO)_2$, and NO_2 were likely produced from reactant O (^{1}D), which was formed from the dissociation of nascent product N_2O. The appearances of the infrared signals of products N_2O, O_3, c-$(NO)_2$, NO, and NO_2 after various periods of irradiation, as shown in Figures 1 and 3(a), support the proposed mechanisms from O_2 dispersed in solid N_2 upon irradiation at 200 nm.

Upon irradiation at 200 nm, precursor O_2 is also pumped through state $B^3\Sigma_u^-$ to excited states $b^1\Sigma_g^+$ and $A'^3\Delta_u$, which

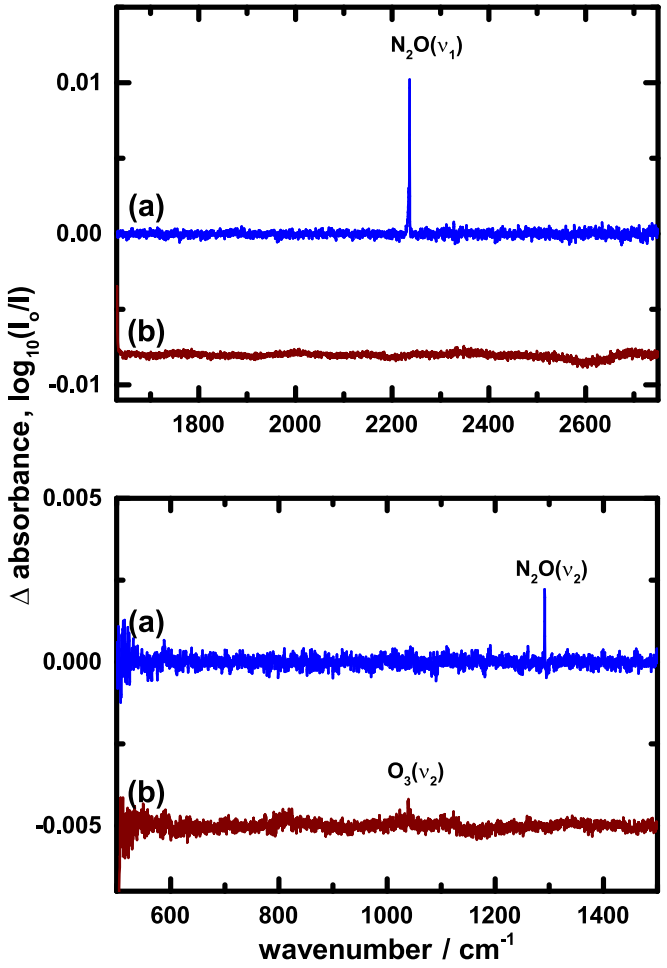

Figure 5. Difference infrared-absorption spectra after irradiation at 200 nm for 40 s near 4 K from (a) O_2 dispersed in solid N_2, 1:500, and (b) O_2 dispersed in solid neon, 1:500. Δabs is the difference of absorbance, $\log_{10}(I_0/I)$.

can relax to the ground state and emit the lines in transitions $b^1\Sigma_g^+ \rightarrow X^3\Sigma_g^-$ and $A'^3\Delta_u \rightarrow X^3\Sigma_g^-$, as shown in Figure 2. During photolysis, the intensities of these emission lines for these two transitions decreased, as displayed in Figure 3(b), indicating the decreasing concentration of precursor O_2.

According to Equation 4(c), nascent product N_2O dissociates to molecular NO and atomic N (^{4}S). Greenblatt & Ravishankara (1990) measured the quantum yield of reaction 4(c) at 193 nm to be 8×10^{-3}. In this photochemical system, the branching reaction to generate atomic N (^{4}S), even with a small ratio, might occur. Upon irradiation at 200 nm, atomic N (^{4}S) can become excited to state ^{2}D, which can then relax to the ground state in a transition $^2\mathrm{D} \rightarrow {}^4\mathrm{S}$ at 521.5 nm. This emission line appeared only during the later stages of irradiation, as displayed in Figure 2. The concentration of N atoms would be expected to increase during the late stages in this photochemical system, consistent with the line at 521.5 nm appearing with a trend as shown in Figure 3(b).

Dinitrogen monoxide was observed toward the core region of the Sagittarius B2 complex with the NRAO 12 m telescope (Ziurys et al. 1994; Halfen et al. 2001). N_2O is thus far the third interstellar molecule detected that contains an N–O bond. Previous work indicated that this molecule is preferentially formed from the neutral–neutral reaction NO+NH→N_2O+H, which has an appreciable rate only for $T > 125$ K. In this work, we recorded that N_2O is the major nascent product from solid O_2 in icy N_2 upon UV photolysis in a cold solid state. Our result indicates that N_2O might form from the reaction of atomic O and molecule N_2 in cold outer space; this reaction route might prevail and requires further consideration in astrophysical environments.

4. Summary

Our analysis of the temporal profiles of products of the photochemical dissociation of solid O_2 in icy N_2 near 4 K with radiation at 200 nm enabled the derivation of a mechanism to explain the formation of products O_3, N, NO, NO_2, N_2O, c-$(NO)_2$, and excited states of O_2 detected through infrared absorption and visible emission spectra. In this work, we found that the nascent product from O_2 dispersed in solid N_2 is N_2O. Our result indicates that the reaction of atomic O and molecule N_2 might be a key reaction for the production N_2O in astrophysical ices. This work enhances our understanding of the evolution of the transformation of oxygen and nitrogen and opens a window for the perception of complicated processes in the solid phase.

NSRRC and Ministry of Science and Technology of Taiwan (grant No. 105-2113-M-213-004-MY3) supported this research. Authors would like to thank the referee for the suggestions.

ORCID iDs

Hsiao-Chi Lu https://orcid.org/0000-0002-0280-1317
Bing-Ming Cheng https://orcid.org/0000-0002-8540-6274

References

Andrews, L., & Spiker, R. C. 1972, JPhCh, 76, 3208
Atkinson, R., Baulch, D. L., Cox, R. A., et al. 1997, JPCRD, 26, 521
Bahou, M., Schriver-Mazzuoli, L., Schriver, A., & Chaquin, P. 1997, CP, 216, 105
Bernstein, M. P., & Sandford, S. A. 1999, AcSpA, 55, 2455
Bernstein, M. P., Sandford, S. A., Allamandola, L. J., et al. 1999, Sci, 283, 1135
Bohn, R. B., Sandford, S. A., Allamandola, L. J., & Cruikshank, D. P. 1994, Icar, 111, 151
Boogert, A., Gerakines, P., & Whittet, D. 2015, ARA&A, 53, 541
Broida, H. P., & Peyron, M. 1960, JChPh, 32, 1068
Chou, S.-L., Lo, J.-I., Lin, M.-Y., et al. 2014, Angew. Chem. Int. Ed., 53, 738
Chou, S.-L., Lo, J.-I., Peng, Y.-C., et al. 2017, ACS Omega, 2, 529
Chou, S.-L., Lo, J.-I., Peng, Y.-C., et al. 2018, PCCP, 20, 7730
Cooper, P. D., Johnson, R. E., & Quickenden, T. I. 2003, P&SS, 51, 183
Cottin, H., Moore, M. H., & Bénilan, Y. 2003, ApJ, 590, 874
Ehrenfreund, P., & van Dishoeck, E. F. 1998, AdSpR, 21, 15
Elsila, J., Allamandola, L. J., & Sandford, S. A. 1997, ApJ, 479, 818
Gerakines, P. A., Schutte, W. A., & Ehrenfreund, P. 1996, A&A, 312, 289
Greenblatt, G. D., & Ravishankara, A. R. 1990, JGR, 95, 3539
Guillory, W. A., & Hunter, C. E. 1969, JChPh, 50, 3516
Halfen, D. T., Apponi, A. J., & Ziurys, L. M. 2001, ApJ, 561, 244
Hudson, R. L., & Moore, M. H. 2001, JGR, 106, 33275
Johnson, R. E., & Jesser, W. A. 1997, ApJL, 480, L79
Johnson, R. E., & Quickenden, T. I. 1997, JGR, 102, 10985
Kaiser, R. I., Maity, S., & Jones, B. M. 2015, Angew. Chem. Int. Ed., 54, 195
Knauth, D. C., Andersson, B.-G., McCandliss, S. R., & Moos, H. W. 2004, Natur, 429, 636
Kramida, A., Ralchenko, Y., & Reader, J. 2016, NIST Atomic Spectra Database, http://www.nist.gov/pml/data/asd.cfm
Linstrom, P. J., & Mallard, W. G. 2016, NIST Chemistry WebBook, http://webbook.nist.gov/chemistry/
Lo, J.-I., Chou, S.-L., Peng, Y.-C., et al. 2014, JESRP, 196, 173
Lo, J.-I., Chou, S.-L., Peng, Y.-C., et al. 2015, ApJS, 221, 20
Lo, J.-I., Chou, S.-L., Peng, Y.-C., et al. 2018, PCCP, 20, 13113
Louis, R. V., St., & Crawford, B., Jr. 1965, JChPh, 42, 857

Materese, C. K., Cruikshank, D. P., Sandford, S. A., et al. 2014, ApJ, 788, 111
Mumma, M. J., & Charnley, S. B. 2011, ARA&A, 49, 471
Muñoz Caro, G. M., & Dartois, E. 2013, Chem. Soc. Rev., 42, 2173
Öberg, K. I. 2016, ChRv, 116, 9631
Okabe, H. 1978, Photochemistry of Small Molecules (New York: Wiley)
Raut, U., Loeffler, M. J., Famá, M., & Baragiola, R. A. 2011, JChPh, 134, 194501
Sandford, S. A., Bernstein, M. P., Allamandola, L. J., Goorvitch, D., & Teixeira, T. C. V. S. 2001, ApJ, 548, 836
Schnepp, O., & Dressler, K. 1965, JChPh, 42, 2482
Sicilia, D., Ioppolo, S., Vindigni, T., et al. 2012, A&A, 543, A155
Sodeau, J. R., & Withnall, R. 1985, JPhCh, 89, 4484
Strobel, D. F., & Shemansky, D. E. 1982, JGR, 87, 1361
Zhu, C., Turner, A. M., Abplanalp, M. J., & Kaiser, R. I. 2018, ApJS, 234, 15
Ziurys, L. M., Apponi, A. J., Hollis, J. M., & Snyder, L. E. 1994, ApJL, 436, L181